
* shenyubing@sinap.ac.cn

The Pedersen model of the passive harmonic double cavity system can be deduced from the expression of the vector relationship and the impedance of the cavity, as shown in Fig.2.

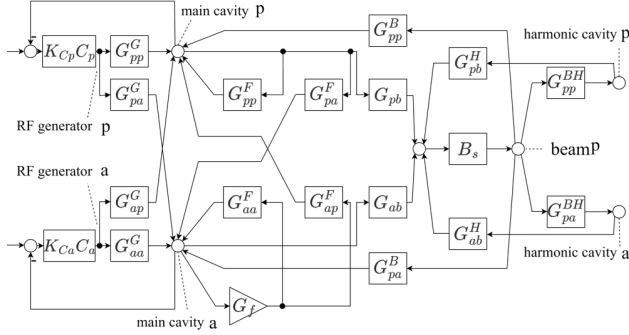


Figure 2: Expanded Pedersen model with passive HHC, ALC, PLL, and DRFB added.

Due to the slow response of tuner loop, only the ALC and PLL are considered in the simulation [8]. Note that this work only includes static beam loading effects. The transfer function that relates the modulation of current excitation to the modulation of cavity voltage signal in HHC is as follows:

$$\begin{cases} G_{pa}^{BP} = \frac{\sigma_p \tan \varphi_H s}{s^2 + 2\sigma_p s + \sigma_p^2 (1 + \tan^2 \varphi_H)} \\ G_{pp}^{BP} = \frac{\sigma_p^2 (1 + \tan^2 \varphi_H) + \sigma_p s}{s^2 + 2\sigma_p s + \sigma_p^2 (1 + \tan^2 \varphi_H)} \end{cases} \quad (3)$$

Where $\sigma = \omega_{rf} / (2Q_L)$ is the cavity damping factor, σ_p is the cavity damping factor of passive HHC. According to the vector relationship

$$\begin{cases} G_{pa}^F = \frac{I_E}{I_T} [G_{aa} \sin(\varphi_F - \varphi_L) + G_{pa} \cos(\varphi_F - \varphi_L)] \\ G_{pp}^F = \frac{I_E}{I_T} [G_{ap} \sin(\varphi_F - \varphi_L) + G_{pp} \cos(\varphi_F - \varphi_L)] \\ G_{pa}^B = \frac{I_B}{I_T} [-G_{aa} \sin(\varphi_s - \varphi_L) - G_{pa} \cos(\varphi_s - \varphi_L)] \\ G_{pp}^B = \frac{I_B}{I_T} [-G_{ap} \sin(\varphi_s - \varphi_L) - G_{pp} \cos(\varphi_s - \varphi_L)] \end{cases} \quad (4)$$

By the same token, we can get transfer functions such as $G_{pa}^G, G_{pp}^G, G_{ap}^F, G_{aa}^F$. $B_s = \Omega_s^2 / (s^2 + \alpha_s \cdot s + \Omega_s^2)$ is the transfer function from the equivalent phase modulation of the total cavity voltage to the phase modulation of the beam current, where Ω_s is the longitudinal oscillation frequency [9]. Main cavity and harmonic cavity can both affect the equivalent phase of the total cavity voltage [10], and the weight of each component is

$$\begin{cases} G_{ab} = [-\cos(\theta_T - \varphi_s) - \sin(\theta_T - \varphi_s) \tan \theta_T] \frac{V_C}{V_T} \\ G_{pb} = [-\sin(\theta_T - \varphi_s) + \cos(\theta_T - \varphi_s) \tan \theta_T] \frac{V_C}{V_T} \\ G_{ab}^P = [\cos(\theta_T - \varphi_H) + \sin(\theta_T - \varphi_H) \tan \theta_T] \frac{V_H}{V_T} \\ G_{pb}^P = [\sin(\theta_T - \varphi_H) - \cos(\theta_T - \varphi_H) \tan \theta_T] \frac{V_H}{V_T} \end{cases} \quad (5)$$

In the DRFB loop, the amplifier must convert a voltage modulation signal into a current modulation signal using $G_f = X/R_L$, where R_L equals the main cavity's load shunt impedance. The ALC and PLL controller functions as a low pass filter that removes the DC component and excludes the carrier frequency portion [11]. Additionally, K_{Ca} and K_{Cp} denote gain, while C_a and C_p represent bandwidth.

$$C_{a,p} = \frac{\omega_{a,p}}{s + \omega_{a,p}} \quad (6)$$

INFLUENCE OF LOOP PARAMETERS ON SYSTEM PERFORMANCE

The Robinson instability calculates the maximum current that a beam can hold within a cavity, which happens when the vectors \vec{V}_G and \vec{I}_B in the diagram are in opposite phases. However, with additional loops, it becomes challenging to portray the instability analysis in the vector diagram due to interactions between the loops. In this case, the new model can compute the open-loop transfer function and plot the Nyquist curve. If the proper controller parameters are in place, the system's poles will not fall in the right half-plane. According to the Nyquist stability criterion, if the open-loop magnitude plot (positive frequency) doesn't cross the left-hand side of the (-1, 0j) point on the real axis, then the closed-loop system is stable with no poles in the right half-plane. The loop delay time T is around 1-2 μs [13] since the klystron's control function has a minor impact on this model's beam dynamics. Since the delay function is approximately $e^{-sT} \approx 1 - sT \approx 1$ and the zero-mode oscillation frequency of SSRF is around 4.8 kHz, the model omits delay for simplicity.

Table 1: High-frequency parameters of SSRF [12] [13]

Energy	3.5GeV
RF frequency	499.654MHz
Harmonic number	720
Radiation loss	1.44MeV
Main RF voltage	4.5-5.4MV
r/Q of third harmonic cavity	88
Harmonic cavity number	3

The shunt impedance of the main cavity is 28.5M Ω , the designed voltage of the main cavity is 5.4 MV. The HHC voltage is approximately 1.8MV under optimal stretching conditions, the detuning frequency can be calculated as 22kHz. The stability can be determined by the gain margin, represented by SC for single cavity and DC for double cavity, as seen in Fig.3 Nyquist plot. Critical stability states are achieved by adjusting the gain and phase shift angle of DRFB as shown in Fig.4.

Setting the phase shift angle in the range of -180° to -300° can make the system more stable. In addition, adding HHC in the stable state will lead to a decrease in stability margin.

Fig. 5 shows that the system is highly unstable when the pre-detuning angle falls within the range of 0-30°. In practice, deviations in the pre-detuning angle are common due to the system's poor loop control capability. To prevent the system from reaching the highly unstable region, a small negative value can be preset for the pre-detuning angle.

After considering ALC and PLL loops, Assume that the initial controller gain is 6 and bandwidth is 1 kHz. The

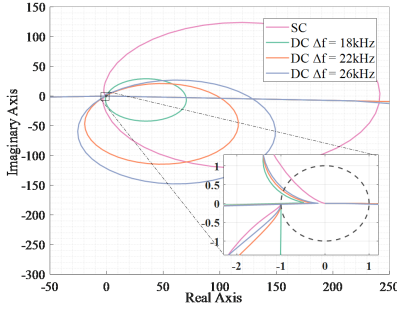


Figure 3: The beam current is 300mA. DRFB is adjusted to achieve the critical stable state, where the curve passes through $(-1, 0j)$, and this state is extended to double cavity system with different detunings, where the system remains in the critical stable state.

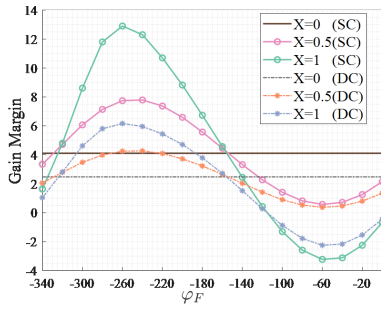


Figure 4: System gain margin versus phase shift angle, that is calculated with single cavity and double cavity, $X=0-1$.

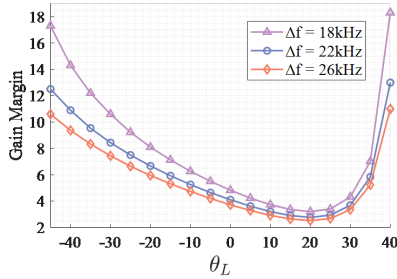


Figure 5: System gain margin versus Pre-detuning angle, that is calculated with HHC detuning frequency 18-26 kHz.

effects of their gain and bandwidth on system stability are discussed separately [14].

By analyzing the Nyquist plot as fig.6, it can be concluded that the stability of various curves can be compared by the phase margin. When the ALC gain increases, the phase margin decreases. However, simulation results have confirmed that variations in PLL gain and controller bandwidth within a certain range do not affect stability margin.

After being converted to an active HHC, the optimal stretching state can be achieved at different beam intensities. Adjusting the HHC transmitter coupling coefficient can meet the optimal coupling, satisfying $\beta_{op} = 1 + P_B/P_H$ [15], and its ALC and PLL controllers are consistent with

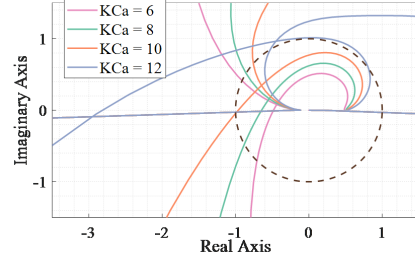


Figure 6: Nyquist plot with gradually increasing amplitude loop gain, system from stable to unstable.

the main cavity. However, it is found that the system is prone to enter an unstable state as shown in Fig.7.

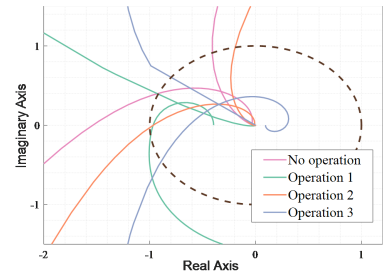


Figure 7: Nyquist plot of the system. operation1: Reduce controller gain to 2 and bandwidth to 500 Hz; operation2: DRFB $X = 1$, $\varphi_F = -260^\circ$; operation3: The coupling coefficient is reduced to one tenth of the optimal coupling.

Three solutions are proposed:

- Reducing the gain and bandwidth of each controller, even if it may result in slower feedback control;
- Using DRFB, but a high feedback gain may result in a decrease in the precision of cavity voltage control or even produce self-excited oscillation in the loop;
- Decreasing the coupling coefficient of the transmitter of the HHC.

CONCLUSION

This article proposes a novel mathematical method based on the Pedersen model to analyze the stability of a harmonic double-cavity system for the first time. The model uses control theory to provide a clear description of the effects of each variable parameter on the stability of the system. Using the SSRF as a case study, it is found that the addition of a passive HHC does not affect the maximum stable current but decreases the stability margin of the system in the stable state. Strategies for optimizing system stability are presented by adjusting the parameters of the pre-detuning angle, DRFB, ALC, and PLL. Moreover, the model is extended to an active HHC system, and it is found that this system is prone to unstable states. Three upgrade proposals for future active harmonic systems are proposed in this paper.

REFERENCES

- [1] L. H. Chang, Ch. Wang, M. C. Lin, and M. S. Yeh, "Effects of the Passive Harmonic Cavity on the Beam Bunch", in *Proceedings of the 2005 Particle Accelerator Conference*, May 2005, pp. 3904-3906. doi: 10.1109/PAC.2005.1591663.
- [2] R. A. Bosch and C. S. Hsue, "Suppression of longitudinal coupled-bunch instabilities by a passive higher harmonic cavity", in *Proceedings of International Conference on Particle Accelerators*, May 1993, pp. 3369-3371 vol.5. doi: 10.1109/PAC.1993.309653.
- [3] K. Ng, "Passive landau cavity for the LNLS light source electron ring", 2000.
- [4] M. G. Minty and R. H. Siemann, "Heavy beam loading in storage ring radio frequency systems", *Nuclear Instruments and Methods in Physics Research Section A: Accelerators, Spectrometers, Detectors and Associated Equipment*, vol. 376, no. 3, pp. 301-318, Jul. 1996, doi: 10.1016/0168-9002(96)00180-5.
- [5] K. W. Robinson, "Stability of beam in radiofrequency system", Cambridge Electron accelerator, Mass., CEAL-1010, Feb. 1964. doi: 10.2172/4075988.
- [6] F. Pedersen, "Beam Loading Effects in the CERN PS Booster", *IEEE Transactions on Nuclear Science*, vol. 22, no. 3, pp. 1906-1909, Jun. 1975, doi: 10.1109/TNS.1975.4328024.
- [7] P. Marchand, "Possible upgrading of the SLS RF system for improving the beam lifetime", *Proceedings of the 1999 Particle Accelerator Conference (Cat. No.99CH36366)*, pp. 989-991 vol.2, 1999, doi: 10.1109/PAC.1999.795424.
- [8] K. Akai, "Stability analysis of rf accelerating mode with feedback loops under heavy beam loading in SuperKEKB", *Phys. Rev. Accel. Beams*, vol. 25, no. 10, 2022, doi: 10.1103/PhysRevAccelBeams.25.102002.
- [9] S. Y. Zhang and W. T. Weng, "Error analysis of acceleration control loops of a synchrotron", *AIP Conference Proceedings*, vol. 255, no. 1, pp. 181-196, May 1992, doi: 10.1063/1.42317.
- [10] S. Belomestnykh, R. Kaplan, J. Reilly, and V. Veshcherevich, "Instability of the RF Control Loop in the Presence of a High-Q Passive Superconducting Cavity", in *Proceedings of the 2005 Particle Accelerator Conference*, May 2005, pp. 2553-2555. doi: 10.1109/PAC.2005.1591178.
- [11] Y.-Y. Xia et al., "Transfer function measurement for the SSRF SRF system", *NUCL SCI TECH*, vol. 30, no. 6, p. 101, May 2019, doi: 10.1007/s41365-019-0612-4.
- [12] X.-Y. Pu et al., "Frequency sensitivity of the passive third harmonic superconducting cavity for SSRF", *NUCL SCI TECH*, vol. 31, no. 3, p. 31, Feb. 2020, doi: 10.1007/s41365-020-0732-x.
- [13] T. Phimsen et al., "Improving Touschek lifetime and synchrotron frequency spread by passive harmonic cavity in the storage ring of SSRF", *NUCL SCI TECH*, vol. 28, no. 8, p. 108, Jun. 2017, doi: 10.1007/s41365-017-0259-y.
- [14] Z.-K. Liu et al., "Modeling the interaction of a heavily beam loaded SRF cavity with its low-level RF feedback loops", *Nuclear Instruments and Methods in Physics Research Section A: Accelerators, Spectrometers, Detectors and Associated Equipment*, vol. 894, pp. 57-71, Jun. 2018, doi: 10.1016/j.nima.2018.03.046.
- [15] A. Chao, "Physics Of Collective Beam Instabilities In High Energy Accelerators", Jan. 1993